Liquid-Phase Hydrogenation of Cinnamaldehyde over Cu-Au/SiO_2 Catalysts

Xiang Yuan
Key Laboratory for Green Chemical Technology of Ministry of Education, School of Chemical Engineering and Technology, Tianjin University, Collaborative Innovation Center of Chemical Science and Engineering, Tianjin 300072, China

Jianwei Zheng and Qian Zhang
School of Chemical and Biomedical Engineering, Nanyang Technological University, Singapore 637459, Singapore

Shuirong Li
Key Laboratory for Green Chemical Technology of Ministry of Education, School of Chemical Engineering and Technology, Tianjin University, Collaborative Innovation Center of Chemical Science and Engineering, Tianjin 300072, China

Yanhui Yang
School of Chemical and Biomedical Engineering, Nanyang Technological University, Singapore 637459, Singapore

Jinlong Gong
Key Laboratory for Green Chemical Technology of Ministry of Education, School of Chemical Engineering and Technology, Tianjin University, Collaborative Innovation Center of Chemical Science and Engineering, Tianjin 300072, China

DOI 10.1002/aic.14522
Published online June 25, 2014 in Wiley Online Library (wileyonlinelibrary.com)

The synthesis, characterization, and application of silica-supported Cu-Au bimetallic catalysts in selective hydrogenation of cinnamaldehyde are described. The results showed that Cu-Au/SiO_2 bimetallic catalysts were superior to monometallic Cu/SiO_2 and Au/SiO_2 catalysts under identical conditions. Adding a small amount of gold (6Cu-1.4Au/SiO_2 catalyst) afforded eightfold higher catalytic reaction rate compared to Cu/SiO_2 along with the high selectivity (53%, at 55% of conversion) toward cinnamyl alcohol. Characterization techniques such as x-ray diffraction, H_2 temperature-programmed reduction, ultraviolet-visible spectroscopy, transmission electron microscopy, Fourier-transform infrared spectra of chemisorbed CO, and x-ray photoelectron spectroscopy were employed to understand the origin of the catalytic activity. A key genesis of the high activity of the Cu-Au/SiO_2 catalyst was ascribed to the synergistic effect of Cu and Au species: the Au sites were responsible for the dissociative activation of H_2 molecules, and Cu^0 and Cu^+ sites contributed to the adsorption-activation of C=C and C=O bond, respectively. A combined tuning of particle dispersion and its surface electronic structure was shown as a consequence of the formation of Au-Cu alloy nanoparticles, which led to the significantly enhanced synergy. A plausible reaction pathway was proposed based on our results and the literature. *AIChE J*, 60: 3300–3311, 2014
Keywords: selective hydrogenation, cinnamaldehyde, α,β-unsaturated aldehyde, Au-Cu alloys, synergistic effect

Introduction

Selective hydrogenation of α,β-unsaturated carbonyl compounds to their corresponding unsaturated alcohols, which dated back to 1925, has been of growing interest because unsaturated alcohols are important intermediates in the production of fine chemicals and pharmaceutical precursors. Particularly, selective hydrogenation of cinnamaldehyde (CALD; Scheme 1) is a representative example of such reactions. Hydrogenation at the C=O bond produces cinnamyl alcohol (CALC), whereas hydrogenation at the C=C bond produces hydrocinnamaldehyde (HALD). Sequential hydrogenation of these two semihydrogenated products leads to hydrocinnamylalcohol (HALC). Nevertheless, selective hydrogenation of C=O bond is difficult because thermodynamics favors C=C hydrogenation over C=O by about 35 kJ mol^{-1}.[1] Homogeneous catalysts such as $RuCl_3$-TPPTS have been successfully used to carry out this reaction.[2,3] Recently, tremendous research efforts have been devoted to designing heterogeneous catalysts especially supported metal nanoparticle catalysts to improve the selectivity toward the desired unsaturated alcohol because heterogeneous catalysts are easier to separate than homogeneous counterparts.

Additional Supporting Information may be found in the online version of this article.

Correspondence concerning this article should be addressed to J. Gong at jlgong@tju.edu.cn (or) Y. Yang at yhyang@ntu.edu.sg.

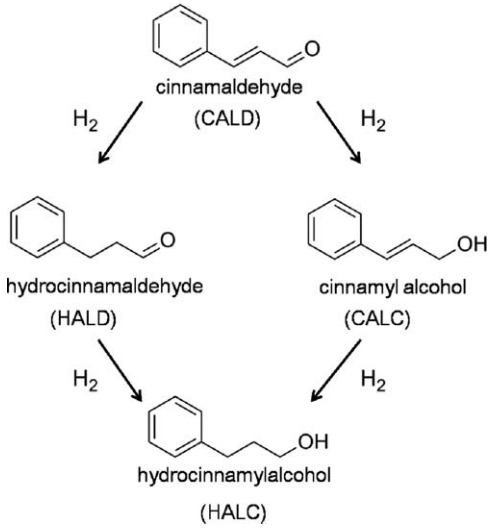

Scheme 1. Reactions involved in the hydrogenation of CALD.

Cu-based catalysts have been intensively investigated primarily due to their high C=O bond hydrogenation selectivity. Volpe and coworkers[4] observed that highly dispersed Cu nanoparticles supported on MCM-48 were selective toward C=O bond activation in CALD hydrogenation (51% of CALC selectivity at 15% of conversion) due to the existence of Cu(I) species. Raju and coworkers[5] reported the significantly high conversion (98%) of furfural and selectivity to furfuryl alcohol (98%) over a Cu/MgO catalyst in the gas-phase hydrogenation, and the superior catalytic performances were attributed to the presence of defective sites at the interface between Cu nanoclusters and MgO surface. In addition, Tsukuda and coworkers[6] developed a size-controlled copper cluster encapsulated within a poly dendrimer, which showed superior catalytic performance in selective hydrogenation of carbonyl and olefin groups. Although Cu-based catalysts are promising in catalyzing selective hydrogenation of α,β-unsaturated carbonyl compounds to their corresponding unsaturated alcohols, the catalytic activity of Cu is usually remarkably poorer than that of noble metals (e.g., Pt, Au, and Pd) due to the weak hydrogen dissociation ability of copper[7,8] (the small adsorption equilibrium constant of Cu), which severely impairs the practical application of Cu catalysts in liquid-phase hydrogenation.

One approach for improving the intrinsic poor catalytic properties of copper catalysts is to add a second metal because bimetallic catalysts frequently exhibit improved catalytic activity and selectivity compared with monometallic catalyst.[9–11] It has been shown that catalysts consisting of Cu-Au,[12–24] Cu-Pt,[25–29] and Cu-Pd[30,31] bimetallic species exhibited higher activity than monometallic copper catalysts in a number of selective catalytic reactions including CO oxidation, propene epoxidation, selective oxidation of alcohols, and water-gas shift reactions. Among these Cu-based bimetallic catalysts, Cu-Au catalysts are unique because introducing Au atoms into Cu nanoparticles affords a facile and feasible way to tune the geometric and electronic properties of Cu-based catalysts, which consequently influences the catalytic performance of copper catalysts. Hutchings and coworkers[20,21] found that Au-Cu alloy nanoparticles were some degree of segregation of copper into the core and gold toward the shell. Shiraishi and coworkers[18] reported that an increase in the density of states for Au upon alloyed with Cu was due to the higher electronegativity of Au compared to Cu. In addition to the improved activity and synergistic effect of Cu-Au bimetallic catalysts in low-temperature CO oxidation and selective oxidation of alcohols,[12–18] the combination of Cu and Au also displayed enhanced catalytic performance in the gas-phase selective hydrogenation. Recently, Fan and coworkers[23] have shown that the Au-Cu alloy nanocatalyst was highly active and selective for the synthesis of methyl glycolate. Yuan and coworkers[24] reported that the Cu-Au/SBA-15 catalyst exhibited remarkable enhancement in its catalytic activity for the hydrogenation of dimethyl oxalate to ethylene glycol.

It is usually accepted that catalysts having an active metal from the Group XI (Cu, Ag, and Au) are less active than those having a metal from other groups, which originates from the electronic structure of the filled d-band of the Group 11 metal. Unlike Cu, gold is an active catalyst when its particle size is in nanosize range.[32] In hydrogenation using diatomic H_2, dissociative chemisorption of H_2 appears to occur primarily on low-coordination Au sites, that is, at corners and edges.[32–35] Therefore, the ability of hydrogen to dissociate and to react on the surface of Au depends on the size of metal nanoparticles. Volpe and coworkers[4] reported that Cu^+ sites were responsible for the adsorption of C=O bond because of the electronic effect in the selective hydrogenation of CALD. These investigations inspire us to design and synthesize the Cu-Au/SiO_2 bimetallic catalysts, which contain the Au and Cu^+ species for liquid-phase selective hydrogenation. Therefore, this article describes the design and application of the silica-supported Cu-Au catalyst (Cu-Au/SiO_2) for the selective hydrogenation of CALD in liquid phase. Detailed investigations on the correlation between catalyst structures and catalytic performances were attempted and a possible mechanism of selective hydrogenation of CALD over Au-Cu alloy nanoparticles supported on inert silica was proposed.

Experimental

Chemicals

$HAuCl_4 \cdot 3H_2O$ (≥49% Au basis, Sigma-Aldrich), $Cu(NO_3)_2 \cdot 3H_2O$(98%, Sigma-Aldrich), $NH_3 \cdot H_2O$ (28.0–30.0% NH_3 basis, Sigma-Aldrich), silica (≥99.5%, 20–45 μm, Silicycle), $H_2PtCl_6 \cdot 6H_2O$ (≥37.5% Pt basis, Sigma-Aldrich), $PdCl_2$ (≥99.9%, Aldrich), CALD (≥99%, Aldrich), *n*-Octane (≥99.0%, Fluka), ethanol (≥99.5%, Sigma-Aldrich), ethyl acetate (EA, ≥99.5%, Acros) were used as received without any further purification.

Catalyst preparation

Silica support was dried in air at 120°C for 24 h prior to the catalyst preparation. The required amounts of 0.01 mol L^{-1} $HAuCl_4$ and 0.1 mol L^{-1} $Cu(NO_3)_2$ solutions, 25 mL of deionized water, and 500 mg of silica were placed in a 100-mL beaker followed by adding 4 mol L^{-1} $NH_3 \cdot H_2O$ dropwise under vigorous stirring at 40°C for 4 h. The initial pH of the suspension was controlled between 11 and 12. The suspension was heated in a water bath to 90°C to allow the evaporation of ammonia. The copper and gold species were successfully deposited on silica when the pH value of the

suspension decreased to 6–7, and the evaporation process was terminated. Upon filtering and washing for several times with deionized water and ethanol, the resultant solids were dried in air at 120°C for 12 h, calcined in air at 350°C for 4 h and then reduced in H_2 at 350°C for 2 h to obtain the final catalyst labeled as xCu-yAu/SiO_2 (x and y denote the weight percentage of Cu and Au, respectively). One should note that the coordination of copper and gold precursors with ammonia was crucial for obtaining the highly dispersed nanoparticles and the reduction in H_2 was necessary to afford the formation of Au-Cu alloy. For comparison purpose, the Cu-Pt/SiO_2 and Cu-Pd/SiO_2 catalysts were also prepared following the same procedure described earlier.

Catalyst characterization

N_2 adsorption–desorption isotherms were measured at −196°C on a Quantachrome Autosorb-6b static volumetric instrument. The samples were degassed at 300°C for 4 h prior to the measurements. The specific surface areas were calculated according to the Brunauer–Emmett–Teller (BET) method. The average pore diameter and pore-size distributions were determined by the Barret–Joyner–Halenda method using the desorption branch. The total pore volume depended on the adsorbed N_2 volume at a relative pressure of approximately 0.99.

Quantitative contents of Cu and Au were measured by inductively coupled plasma optical emission spectroscopy (ICP-OES) on a Thermo Elemental IRIS Intrepid II XSP. The sample was treated by aqua regia at 90°C for 30 min, and the resultant solution was heated until it evaporated. The residue was diluted with 5% HNO_3 and filtrated to a 25-mL volumetric flask before ICP-OES measurements.

Powder x-ray diffraction (XRD) patterns were acquired on a Rigaku Ultima IV diffractometer equipped with Cu Kα radiation ($\lambda = 1.54056$ Å and scan rate of 2°/min). The diffraction peaks were identified by referring to the JCPDS database.

H_2 temperature-programmed reduction (H_2-TPR) was carried out on a Micromeritics Autochem II 2920. The as-calcined catalyst (100 mg) was loaded into quartz and dried in an argon stream at 120°C for 1 h before the reduction. The catalyst was then heated in 30 mL min^{-1} of 5%H_2-Ar at a heating rate of 10°C/min up to 800°C. A thermal conductivity detector was used to determine the amount of hydrogen consumption during the run.

Transmission electron microscopy (TEM) observation was conducted to characterize the morphology of catalysts using a JEM-2100F transmission electron microscope at 200 kV. The catalyst powders were lightly ground and ultrasonically dispersed in ethanol at room temperature. The as-obtained solution was then dropped into copper grids supported on holey carbon films.

Ultraviolet-visible spectroscopy (UV-Vis) spectra of as-reduced catalysts were taken on a Shimazu UV-2550. On reduction, the as-reduced catalysts were cooled to room temperature in N_2 and directly produced for the UV-Vis DRS measurement.

X-ray photoelectron spectroscopy (XPS) and Auger electron spectroscopy (AES) were carried out on a Quantum 2000 Scanning ESCA Microprob instrument equipped with an Al Kα x-ray radiation source ($E = 1486.6$ eV). The catalysts were carefully collected and sealed under the protection of Ar atmosphere after reduced in H_2 at 350°C for 2 h. The samples were pressed into a thin disk in a glove box, and then transferred into the XPS chamber without exposure to air. All spectra were recorded at room temperature and the binding energy (BE) was referred to 284.5 eV for C_{1s} peak, as shown in the XPS handbook. The concentration of each element was calculated from the area of the corresponding peak and calibrated with the Wagner sensitivity factor.

Fourier-transform infrared (FTIR) spectra of chemisorbed CO on activated catalysts were collected on a Nicolet 6700 spectrometer using a stainless steel cell connected to a gas-dosing and evacuation system. In a typical procedure, 30 mg of as-calcined catalyst was compressed into a 13-mm diameter self-supporting wafer and carefully loaded into *in situ* cell equipped with ZnSe windows. The catalyst wafer was reduced under a flow of H_2 (30 mL/min) at 350°C for 2 h followed by purging He for 1 h to completely remove the chemisorbed hydrogen species, and then cooled to 30°C for collecting the background spectrum. Subsequently, the sample was exposed to a flowing of CO (10 mL/min) at 30°C for 30 min. IR spectra were collected after purging He (30 mL/min) for 30 min and referenced to the background spectrum of reduced catalyst. Four scans were averaged using a resolution of 4 cm^{-1}.

Catalyst testing

Hydrogenation of CALD was carried out in a 40-mL stainless steel reactor with Teflon liner (Parr 4950, controller 4843). A certain amount of catalyst (70 mg), 0.2 g of CALD (1.5 mmol), and 15 mL of EA were added into the reactor. *n*-Octane (38 μL, 0.233 mmol) was added as an internal standard. On purged with H_2 (~1.0 MPa) five times, the autoclave was pressurized to a desired H_2 pressure (e.g., 2.0 MPa) at room temperature. When the autoclave was heated to the reaction temperature (e.g., 100°C), the mechanical stirring (900 rpm) was switched on and zero reaction time was taken. To eliminate the external mass-transfer limitation, preliminary experiments were performed using varying stirring speeds (in the range of 600–1200 rpm). The results showed that CALD conversion was constant when the stirring speed was above 900 rpm. Thus, the stirring speed was set at 900 rpm for all the experiments in this study. The absence of mass-transfer effect on the reaction rate was also confirmed by changing the catalyst mass (25–90 mg) for the reaction using 6Cu-1.4Au/SiO_2 catalyst, as shown in Supporting Information Figure S1. An ice-water bath was used to cool the autoclave at the end of each reaction. The catalyst powder was filtered off, and the filtrate was analyzed using a gas chromatograph (Agilent, 6890 N) equipped with a HP-5 column (Agilent) and a flame ionization detector.

Initial reaction rate is defined as

$$\text{Initial rate} = \frac{X_{\text{CALD}} \times n_{\text{CALD, start}}}{m_{\text{catal}} \times t}$$

X_{CALD}, $n_{\text{CALD,start}}$, m_{catal}, and t are the conversion of CALD, molar of CALD, mass of catalyst, and reaction time, respectively.

Results

Physicochemical properties of catalysts

Table 1 summarizes the chemical composition and textural properties of a series of xCu-yAu/SiO_2 catalysts with fixed Cu loading (6 wt %) and varied Au loading (0–1.9 wt %).

Table 1. Physicochemical Properties of xCu-yAu/SiO_2 Catalysts

Catalyst	Cu Loading (wt %)[a]	Au Loading (wt %)[a]	Cu/Au Atomic Ratio		S_{BET} ($m^2\ g^{-1}$)	D_{pore} (nm)	V_{pore}[b] ($cm^3\ g^{-1}$)	d_{TEM} (nm)
			By ICP	By XPS				
SiO_2	0	0	–	–	415	7.2	0.74	–
6Cu/SiO_2	5.71	0	∞	∞	247	10.4	0.64	2.4 ± 0.5
6Cu-0.4Au/SiO_2	5.81	0.34	52.9:1	17.9:1	270	9.7	0.65	2.8 ± 0.5
6Cu-0.9Au/SiO_2	5.67	0.88	20.0:1	8.3:1	254	9.9	0.63	3.1 ± 0.6
6Cu-1.4Au/SiO_2	5.89	1.19	15.3:1	4.1:1	249	10.3	0.64	3.6 ± 0.4
6Cu-1.9Au/SiO_2	6.05	1.67	11.2:1	2.6:1	243	10.7	0.65	4.3 ± 0.7
2Au/SiO_2	0	1.86	0	0	302	9.8	0.74	5.4 ± 0.6

[a]Metal loading determined by ICP-OES.
[b]Obtained from $P/P^0 = 0.99$.

The actual metal loadings are measured by ICP and they are close to the nominal values. The BET surface area of SiO_2 is 415 $m^2\ g^{-1}$, and the pore size is 7.2 nm. The BET surface areas and average pore diameters range from 243 to 302 $m^2\ g^{-1}$ and 9.7 to 10.7 nm with varying Cu/Au ratios, respectively. Supporting Information Figure S2 shows the N_2 adsorption–desorption isotherms (Supporting Information Figure S2A) and the pore-size distribution curves (Supporting Information Figure S2B) of *x*Cu-*y*Au/SiO_2 catalysts. The hysteresis loop of the N_2 adsorption–desorption does not change significantly when the Cu/Au ratio changed. All these catalysts have comparable surface areas and pore diameters, indicating that introducing Cu and Au did not significantly affect the porosity of the silica support.

X-ray diffraction

Figure 1 presents XRD patterns of the reduced *x*Cu-*y*Au/SiO_2 catalysts (curves a-f), the as-calcined 6Cu-1.4Au/SiO_2 sample (curve g), 6Cu/SiO_2 and 6Cu-1.4Au/SiO_2 catalysts reused for three runs (curve h, i). No obvious diffraction peaks except for a minor peak corresponding to Cu_2O (111) appears at $2\theta = 36.6°$ can be observed on the Cu/SiO_2 sample, implying that the copper nanoparticles were highly dispersed on the silica support. Au/SiO_2 shows four diffraction peaks at $2\theta = 38.2$, 44.6, 64.7, and 77.5°, and they are indexed as Au (111), (200), (220), and (311) reflections, respectively. The Cu-Au/SiO_2 samples peaks shift toward lower 2θ value [close to Au (111)] with the Au addition, and the peaks shift the greatest amount with the highest nominal content of Au (6Cu-1.9Au/SiO_2), indicating the formation of an Au-Cu alloy. Moreover, the calcined 6Cu-1.4Au/SiO_2 sample (curve g) shows the diffraction peaks at the same position as the Au/SiO_2 catalyst (curve f). On reduction of this catalyst in H_2 at 350°C (curve d), the diffraction peaks become broader and shift toward higher 2θ value, suggesting that the H_2 reduction step is indispensable for the formation of Au-Cu alloy and the particle size of Au-Cu alloy becomes smaller after reduction. In addition, the reused catalysts (curve h, i) show the diffraction peaks at the same position as those of fresh samples (curve a, d), respectively.

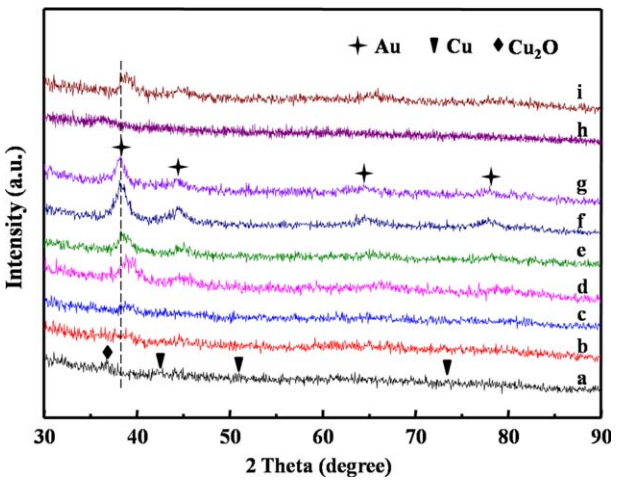

Figure 1. XRD patterns of the *x*Cu-*y*Au/SiO_2 catalysts.

(a) 6Cu/SiO_2, (b) 6Cu-0.4Au/SiO_2, (c) 6Cu-0.9Au/SiO_2, (d) 6Cu-1.4Au/SiO_2, (e) 6Cu-1.9Au/SiO_2, (f) 2Au/SiO_2, (g) 6Cu-1.4Au/SiO_2-unreduced (calcined), (h) 6Cu/SiO_2 reused for three runs, and (i) 6Cu-1.4Au/SiO_2 reused for three runs. [Color figure can be viewed in the online issue, which is available at wileyonlinelibrary.com.]

H_2 temperature-programmed reduction

H_2-TPR technique was used to investigate the effect of Au species on the H_2 activation of Cu-Au bimetallic catalyst. Figure 2 displays the TPR profiles of as-calcined *x*Cu-*y*Au/SiO_2 catalysts. For the Au/SiO_2 catalyst, there is no signal for the reduction of oxidized gold species as the gold species would exist as Au^0 when the catalyst was calcined in air at 350°C, as is confirmed by XRD results. Comparatively, the Cu/SiO_2 and Cu-Au/SiO_2 samples possess a single reduction peak centered at 227 and 222°C, respectively. According to XRD data for analogous samples reduced in H_2 at 350°C, this reduction peak could be assigned to the reduction of the well-dispersed CuO to metallic Cu and Cu_2O.[36] Although the content of Cu

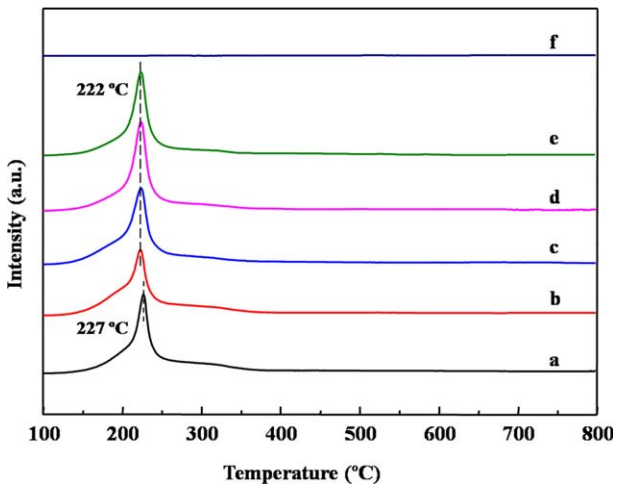

Figure 2. H_2-TPR profiles of the as-calcined *x*Cu-*y*Au/SiO_2 catalysts.

(a) 6Cu/SiO_2, (b) 6Cu-0.4Au/SiO_2, (c) 6Cu-0.9Au/SiO_2, (d) 6Cu-1.4Au/SiO_2, (e)6Cu-1.9Au/SiO_2, and (f) 2Au/SiO_2. [Color figure can be viewed in the online issue, which is available at wileyonlinelibrary.com.]

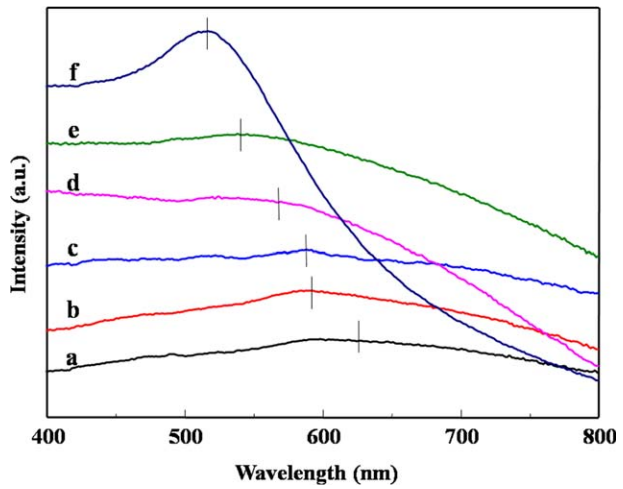

Figure 3. UV-Vis spectra of the *x*Cu-*y*Au/SiO_2 catalysts.

(a) 6Cu/SiO_2, (b) 6Cu-0.4Au/SiO_2, (c) 6Cu-0.9Au/SiO_2, (d) 6Cu-1.4Au/SiO_2, (e) 6Cu-1.9Au/SiO_2, and (f) 2Au/SiO_2. [Color figure can be viewed in the online issue, which is available at wileyonlinelibrary.com.]

in each catalyst is similar, the TPR profiles show that the reduction peak width at half height becomes broader with the increasing addition of Au. One should note that the presence of gold leads to a lowering of the reduction temperature. One probable explanation is that gold in the sample could activate H_2 and supply active H-species, resulting in CuO reduced at relatively low temperatures. For example, Lee and coworkers[37] have observed that the reduction of copper oxides promoted by the presence of Pd metal. The same issue was also discussed in the Pt-Cu bimetallic system.[38] As for the Au-Cu bimetallic system, as the hydrogen dissociation ability of Au is relatively weak as compared to that of Pt and Pd, the promotion in the reduction of CuO is less significant. Limited peak shift was observed in the H_2-TPR profiles of Au-Cu/TiO_2 as reported by Medina and coworkers[19] and also observed in our work. Therefore, the introduction of Au species into the Cu/SiO_2 catalyst enhances H_2 activation ability.

UV-Vis spectra

Figure 3 shows UV-Vis spectra of the reduced *x*Cu-*y*Au/SiO_2 samples. Au/SiO_2 presents a single and strong absorption peak at 530 nm due to the surface plasma resonance of gold nanoparticles, and Cu/SiO_2 shows a relative weak absorption peak at 630 nm. These results are consistent with earlier reports.[20,21] For the Cu-Au/SiO_2 catalysts with different Au loadings, only one absorption peak can be observed at the intermediate position between that of the monometallic Cu/SiO_2 and Au/SiO_2 catalysts. This result confirms that the metal particles are not a mixture of separate gold and copper particles, but composed of Au-Cu alloy nanoparticles. Moreover, this absorption peak displays a blue shift with increased Au content, implying the changed electronic structure as the optical properties of metal nanoparticles depend on the collective oscillation of conduction electrons (surface plasmon resonance) on interaction with an incoming electromagnetic field.[39]

Surface morphology

TEM images in Figure 4 show that all the nanoparticles are uniformly distributed on the surfaces of the SiO_2 support. The average particle size of copper in the Cu/SiO_2 is about 2.4 ± 0.5 nm, and gold particle size of the Au/SiO_2 is about 5.4 ± 0.6 nm. Interestingly, on alloying Cu with Au, the alloy particle size becomes smaller than that of monometallic Au/SiO_2 catalyst.

Further examination on the 6Cu-1.4Au/SiO_2 catalyst with HRTEM (Figures 4g, h) reveals that the *d*-spacing in a single particle is about 2.22 Å, which is remarkably smaller than that of monometallic Au(111) (2.36 Å), but larger than that of the monometallic Cu(111) (2.09 Å). The result is in good agreement with the value calculated from the XRD of the Au-Cu alloy, and it again confirms that the metal particles are not a mixture of separate gold and copper particles, but composed of Au-Cu alloy.

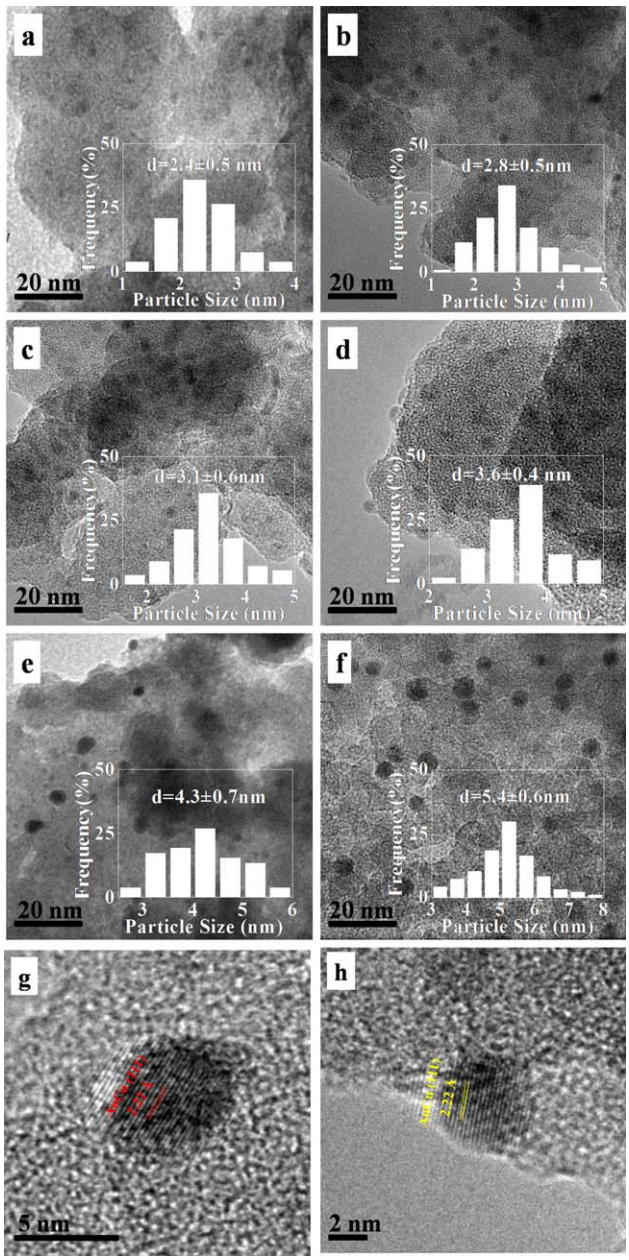

Figure 4. TEM and HRTEM images of the *x*Cu-*y*Au/SiO_2 catalysts.

(a) 6Cu/SiO_2, (b) 6Cu-0.4Au/SiO_2, (c) 6Cu-0.9Au/SiO_2, (d) 6Cu-1.4Au/SiO_2, (e) 6Cu-1.9Au/SiO_2, (f) 2Au/SiO_2, and (g, h) 6Cu-1.4Au/SiO_2. [Color figure can be viewed in the online issue, which is available at wileyonlinelibrary.com.]

Table 2. Surface Cu Component of Reduced Catalysts Based on Cu LMM Deconvolution

Catalyst	BE_{Au}[a] (eV)	BE_{Cu}[b] (eV)	KE (eV)[c] Cu^+	KE (eV)[c] Cu^0	$A_{Cu^+}/_{Cu^0}$[d]
$6Cu/SiO_2$	–	932.4	914.3	918.5	0.75
$6Cu\text{-}0.4Au/SiO_2$	83.7	932.6	914.3	918.5	1.0
$6Cu\text{-}0.9Au/SiO_2$	83.8	932.6	914.3	918.5	0.89
$6Cu\text{-}1.4Au/SiO_2$	83.8	932.6	914.3	918.5	0.82
$6Cu\text{-}1.9Au/SiO_2$	83.8	932.6	914.3	918.5	0.79
$2Au/SiO_2$	84.0	–	914.3	918.5	–

[a]Binding energy of Au $4f_{7/2}$.
[b]Binding energy of Cu $2p_{3/2}$.
[c]Kinetic energy.
[d]Peaks area ratio between Cu^+ and Cu^0 by deconvolution of Cu LMM AES spectra.

Chemical states

Further efforts are made to understand the Cu-Au nanoparticle structure and electronic properties by conducting XPS characterization. Table 1 shows that the surfaces of all samples are enriched in Au compared with the bulk composition. For example, the surface Cu/Au molar ratio of 6Cu-1.4Au/SiO_2 is 4:1 (XPS analysis), but the molar ratio of the total amounts of Cu and Au in the catalyst is 15:1 (ICP analysis). XPS spectra of Cu 2p and Au 4f are also collected and the quantitative results are included in Table 2. The BEs of Au $4f_{7/2}$ (Au/SiO_2) and Cu $2p_{3/2}$ (Cu/SiO_2) are 84.0 and 932.4 eV, respectively, which are consistent with that of metallic Au and Cu species. XPS analysis further shows that the Cu_{2p} BE of the Cu-Au/SiO_2 bimetallic catalysts shifts to a higher energy value compared with that of the monometallic Cu/SiO_2 and Au_{4f} BE shifts to a lower energy value compared with that of the monometallic Au/SiO_2 (Figure 5A), implying that the Au species have an increase in the density of states when alloyed with Cu. The change in BE values suggests that alloying Cu with Au results in the electronic interaction and a net charge flow between Cu and Au.

AES measurement was carried out to determine the amount of Cu^0 and Cu^+ species in the reduced catalysts. In the Cu LMM AES spectra as shown in Figure 5B, asymmetry and broad peaks are observed and deconvoluted into two symmetric peaks centered at 918.5 and 914.3 eV, corresponding to Cu^0 and Cu^+ species, respectively. As shown in the deconvolution results (Table 2), the molar ratio of surface Cu^+/Cu^0 species of Cu-Au/SiO_2 catalysts are higher than that of Cu/SiO_2 catalyst, which may be related to the electronic interaction between Cu and Au.[24] However, the molar ratio of surface Cu^+/Cu^0 shows change in a volcano-shaped trend. With Au incorporation into the Cu/SiO_2 sample, the molar ratio of surface Cu^+/Cu^0 species first increases and subsequently decreases gradually, which could be ascribed to the increase of Au concentration on the catalysts surfaces.

FTIR spectra of CO adsorbed on catalysts

FTIR investigation of CO chemisorptions is useful to identify the surface species of supported Cu-based catalysts. All catalysts were activated in H_2 at 350°C for 2 h prior to CO adsorption at room temperature for 0.5 h. Figure 6 displays the FTIR spectra of CO adsorption on the reduced *x*Cu-*y*Au/SiO_2 catalysts. There is no observable IR band for chemisorbed CO species can be found on the Au/SiO_2 between 2300 and 2000 cm^{-1}, while a single band at 2123 cm^{-1} is present on Cu/SiO_2 and Cu-Au/SiO_2. It have been shown that CO adsorption on either Cu^0 or Cu^{2+} was very weak and easily removed by purging with inert gas at room temperature.[15,40] In addition, the assignment of CO adsorptions onto Cu^0, Cu^+, and Cu^{2+} surfaces has been well-documented in previous work.[24,41–43] Therefore, the adsorption band observed on the Cu/SiO_2 and Cu-Au/SiO_2 must be due to the CO adsorbed on Cu^+ species. The result confirms that the Cu^+ species exist on the surface of the metallic nanoparticles. Moreover, the varied strength of CO-adsorbed peaks of *x*Cu-*y*Au/SiO_2 is consistent with the molar ratio of surface Cu^+/Cu^0 species.

Selective hydrogenation of CALD

Effect of Au Entities in Cu-Au/SiO_2. Table 3 shows the effect of Au loadings in the Cu-Au/SiO_2 catalysts on the catalytic performance for selective hydrogenation of CALD. The Cu/SiO_2 catalyst shows the same selectivity toward the formation of CALC and HALD and produces a low CALD conversion (~16%) in a reaction period of 3 h under the

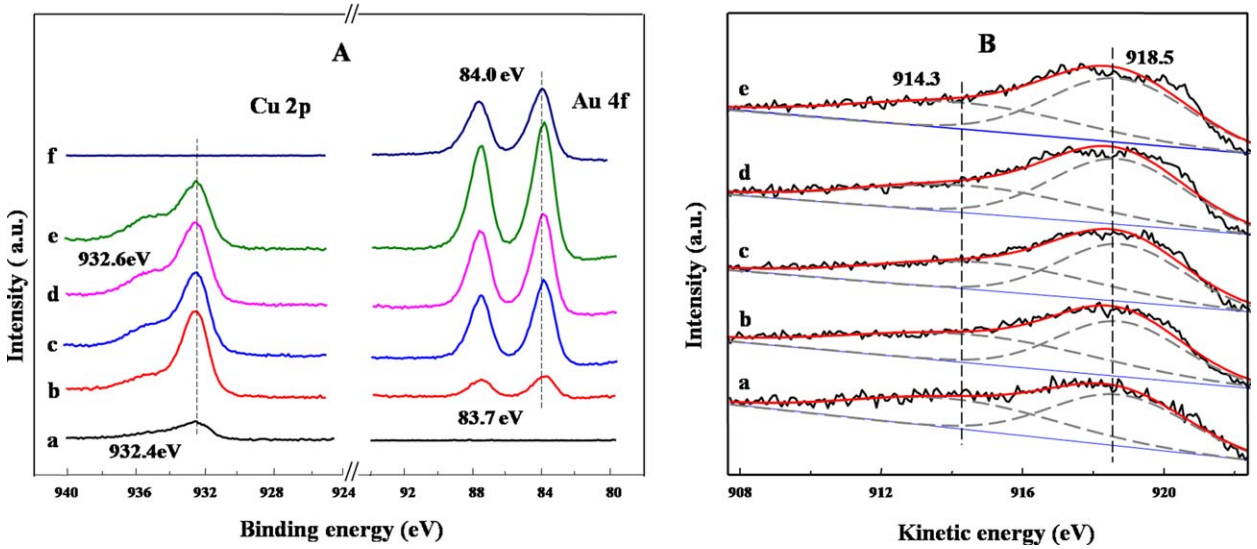

Figure 5. (A) Cu 2p and Au 4f XPS and (B) Cu LMM AES spectra of the *x*Cu-*y*Au/SiO_2 catalysts: (a) 6Cu/SiO_2, (b) 6Cu-0.4Au/SiO_2, (c) 6Cu-0.9Au/SiO_2, (d) 6Cu-1.4Au/SiO_2, (e)6Cu-1.9Au/SiO_2, and (f) 2Au/SiO_2.

[Color figure can be viewed in the online issue, which is available at wileyonlinelibrary.com.]

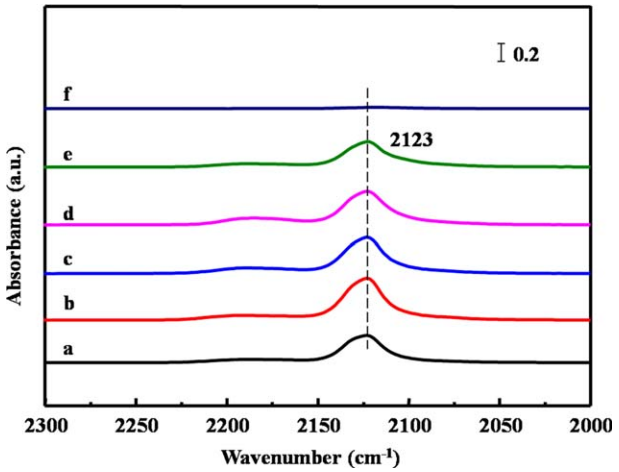

Figure 6. *In situ* FTIR spectra of chemisorbed CO on the *x*Cu-*y*Au/SiO2 catalysts.

(a) $6Cu/SiO_2$, (b) $6Cu\text{-}0.4Au/SiO_2$, (c) $6Cu\text{-}0.9Au/SiO_2$, (d) $6Cu\text{-}1.4Au/SiO_2$, (e) $6Cu\text{-}1.9Au/SiO_2$, and (f) $2Au/SiO_2$. [Color figure can be viewed in the online issue, which is available at wileyonlinelibrary.com.]

reaction conditions (100°C, $P_{H2} = 2.0$ MPa). Au/SiO_2 catalyst shows a high selectivity toward the formation of HALD (84%). Alloying a small amount of Au (Au loading = 0.4%) with Cu nanoparticles elevates the CALD conversion to 31%, a twofold increment in the same duration of reaction (3 h). Further increasing the gold loading to 0.9 and 1.4, the CALD conversions are improved to 48 and 55%, respectively. Nevertheless, the conversion of CALD decreases to 42% with further increasing the Au contents. For a comparison, $6Cu\text{-}0.8Pd/SiO_2$ and $6Cu\text{-}1.4Pt/SiO_2$ catalysts are attempted in this reaction under the same conditions. Improved activities are observed over these two catalysts, but the selectivity to CALC over $6Cu\text{-}0.8Pd/SiO_2$ and $6Cu\text{-}1.4Pt/SiO_2$ are only 13 and 36%, respectively.

To compare the catalytic activity of these xCu-yAu/SiO_2 catalysts in the absence of deactivation, the CALD conversion level is controlled in the range of 10–20% by adjusting the duration of the catalytic reaction (Table 4). The CALD conversion data are then used to calculate the reaction rates by CALD consumption according to the mass of catalyst. The reaction rate for Cu/SiO_2 is as low as 1.1 mmol h^{-1} $g_{cal}{}^{-1}$ and is enhanced to eightfold higher for $6Cu\text{-}1.4Au/SiO_2$ catalyst. The product selectivity is also found affected slightly by adding Au entities. Introducing a small amount of Au into the catalyst increases the selectivity to CALC from 49 to 58%. However, the selectivity to CALC decreases with further increasing the gold loading. For a comparison, the mechanical mixture of Cu/SiO_2 and Au/SiO_2 catalyst is employed, which exhibits negligible catalytic activity enhancement. These results indicate that the Au-Cu alloys rather than physical mixing of Cu and Au nanoparticles enhance the performance of CALD hydrogenation.

To confirm that no Cu or Au leached into the filtrate, ICP-OES technique was used to measure the contents of Cu and Au over the reused $6Cu/SiO_2$ and $6Cu\text{-}1.4Au/SiO_2$ catalysts (Supporting Information Table S1). The absence of Cu and Au ions in the filtrate was double-checked using ICP analysis (detection limit: 0.10 ppm). Furthermore, the $6Cu/SiO_2$ and $6Cu\text{-}1.4Au/SiO_2$ were recovered by filtering the solid from the liquid phase after reaction, respectively. The recovered catalysts were washed with ethanol and water for several times, dried in air at 120°C for 12 h, reduced again in H_2 at 350°C for 2 h and then reused as catalysts for the next run under the same conditions. After reused three runs, the catalysts were stable and maintained their activity and selectivity (Table 3). XRD results (Figure 1) and TEM images (Supporting Information Figure S3) of $6Cu/SiO_2$ and $6Cu\text{-}1.4Au/SiO_2$ after the reuse reveal that the average diameter and size distribution of the metal particles are similar to the corresponding fresh catalysts, and that no aggregation of the used metal particles is apparent.

Effect of Reaction Temperature and H_2 Pressure. It is well known that the chemoselectivity in hydrogenation of α,β-unsaturated aldehydes depends significantly on the reaction temperature and H_2 Pressure.[44,45] Cu/SiO_2 and $6Cu\text{-}1.4Au/SiO_2$ catalysts are attempted to show the effects of reaction temperature and H_2 pressure on the hydrogenation of CALD. To minimize the deviation in measuring the catalytic rates, CALD conversion levels in these experiments are also restrained to 16–21% by adjusting the duration of the reaction, and the catalytic results are shown in Table 5. Increasing the reaction temperature from 100 to 130°C for Cu/SiO_2 and from 90 to 120°C for $6Cu\text{-}1.4Au/SiO_2$ results in shorter reaction time period for achieving a certain CALD conversion. The reaction rate increases fivefold for both Cu/SiO_2 and $6Cu\text{-}1.4Au/SiO_2$ catalysts when the reaction temperature is elevated by 30°C. The Arrehenius plots derived from reaction rates over Cu/SiO_2 and $6Cu\text{-}1.4Au/SiO_2$ catalysts are shown in Figure 7. The corresponding apparent activation energy (E_a) is 62.2 ± 2.1 kJ mol^{-1} for Cu/SiO_2 and 58.2 ± 2.6 kJ mol^{-1} for $6Cu\text{-}1.4Au/SiO_2$ catalyst.

In addition, these two catalysts respond similarly to the reaction temperature with regard to the product selectivity. When increasing the reaction temperature from 100 to 130°C, the CALC selectivity over Cu/SiO_2 catalyst decreases from 49 to 37%. The CALC selectivity over $6Cu\text{-}1.4Au/SiO_2$ catalyst decreases from 55 to 43% when the reaction temperature is elevated from 90 to 120°C. The higher selectivity toward HALD at higher reaction temperature can be explained by a significantly higher barrier in C=O bond activation, as the dissociation energy of C=O bond (174 kcal mol^{-1}) is much higher than that of the C=C bond (141 kcal mol^{-1}).[46] Preferred hydrogenation of the C=C bond of crotonaldehyde at higher reaction temperatures was previously observed over Au/Mg_2AlO catalyst.[47]

Table 3. Catalytic Results of CALD Hydrogenation[a]

Catalyst	Time (min)	Conversion (%)	Selectivity (%)		
			CALC	HALD	HALC
SiO_2	180	0	0	0	0
$6Cu/SiO_2$	180	16	49	49	2
$6Cu\text{-}0.4Au/SiO_2$	180	31	56	38	6
$6Cu\text{-}0.9Au/SiO_2$	180	48	55	37	8
$6Cu\text{-}1.4Au/SiO_2$	180	55	53	38	9
$6Cu\text{-}1.9Au/SiO_2$	180	42	51	40	9
$2Au/SiO_2$	180	10	15	84	1
$6Cu+1.9Au/SiO_2$	180	23	37	60	3
$6Cu\text{-}0.8Pd/SiO_2$	30	38	13	67	20
$6Cu\text{-}1.4Pt/SiO_2$	30	58	36	56	8
$6Cu/SiO_2$[b]	180	15	50	48	2
$6Cu\text{-}1.4Au/SiO_2$[b]	180	53	54	38	8

[a]Reaction temperature = 100°C; $P_{H2} = 2$ MPa; CALD = 1.5 mmol; stirring speed = 900 rpm.
[b]Results for the third run.

Table 4. Catalytic Results of CALD Hydrogenation[a]

Catalyst	Time (min)	Conversion (%)	Selectivity (%)			Initial rate[b]
			CALC	HALD	HALC	
$6Cu/SiO_2$	180	16	49	49	2	1.1
$6Cu\text{-}0.4Au/SiO_2$	60	13	58	41	1	2.8
$6Cu\text{-}0.9Au/SiO_2$	30	19	56	43	1	8.1
$6Cu\text{-}1.4Au/SiO_2$	30	20	52	46	2	8.6
$6Cu\text{-}1.9Au/SiO_2$	30	13	50	49	1	5.6
$2Au/SiO_2$	180	10	15	84	1	0.7

[a]Reaction temp = 100°C; P_{H2} = 2 MPa; CALD = 1.5 mmol; stirring speed = 900 rpm.
[b]Initial reaction rate, mmol h^{-1} g_{cat}^{-1}.

The effect of hydrogen pressure on CALD hydrogenation over Cu/SiO_2 and $6Cu\text{-}1.4Au/SiO_2$ catalysts was also investigated. In liquid-phase hydrogenation reaction, the rates and selectivity should be measured using the dissolved concentration of hydrogen. However, the dissolved concentration of hydrogen is influenced by many factors that are hard to be measured precisely. Futhermore, according to Henry's law, at a constant temperature, the amount of dissolved concentration of hydrogen is directly proportional to the partial pressure of hydrogen. Therefore, we used the partial pressure of hydrogen instead of the dissolved concentration of hydrogen to explain the experimental phenomena.[48,49] Figure 8 lists catalytic results as well as the reaction rates by CALD consumption. Increasing P_{H2} from 1 to 4 MPa, the reaction rate over Cu/SiO_2 catalyst increases threefold, while the same increase in H_2 pressure for the reaction over the $6Cu\text{-}1.4Au/SiO_2$ catalyst affects a fivefold increase in the reaction rate. As shown in Figure 8, both the reaction rates over Cu/SiO_2 and $6Cu\text{-}1.4Au/SiO_2$ catalysts are proportional to the H_2 partial pressure, which indicates that the apparent H_2 reaction order of Cu/SiO_2 and $Cu\text{-}Au/SiO_2$ are close to first order. The product selectivity remain essentially unchanged with the H_2 pressure changing for both Cu/SiO_2 and $6Cu\text{-}1.4Au/SiO_2$ catalysts. The negligible effect of the hydrogen pressure on the product selectivity may be ascribed to the noncompetitive adsorption of hydrogen with C═O bond and C═C bond. We also note that the steric hindrance of the phenyl group protects the C═C bond from adsorbing to the surface, which could also be a possible factor in affecting the product selectivity.

Discussion

Cu-Au bimetallic catalysts have been reported to exhibit their excellent performance in the industrially important oxidation reactions, but reports on hydrogenation reactions are limited.[20] Particularly, the origin of the promotional effect on bimetallic catalysts is still unclear and sometimes even controversial. In the present study, the Cu-Au bimetallic catalyst is active for the liquid-phase selective hydrogenation reaction. Under the same reaction condition, supported monometallic Cu and Au exhibit poor activity, but a significant improvement occurs when the Cu and Au species are fused with each other to form alloy on the support. The reaction rate for Cu/SiO_2 is enhanced to eightfold higher by adding appropriate amounts of Au, showing that Au considerably improves Cu catalytic activity.

During the synthesis of catalyst, the Cu and Au precursors are homogeneously mixed and precipitated on the SiO_2 support. On the calcination treatment, the copper is oxidized, and the gold exists as Au^0. Thus, it can be inferred that the as-calcined bimetallic nanoparticles are composed of CuO and Au^0. On the subsequent reduction pretreatment in hydrogen flow, CuO is reduced into Cu^+ and Cu^0. The Cu^+ species on the metallic particle surface plays an important role in selective hydrogenation of C═O,[50] while the Cu^0 fuses with Au^0 and finally forms a nanosized Au-Cu alloy phase, which is confirmed by various characterization techniques. The formation of Au-Cu alloy laid the foundation for the synergy between Cu and Au.

The catalytic performance of Au-Cu alloy catalysts are superior to that of the monometallic Cu and Au catalysts, and the catalytic activity of Au-Cu alloy can be tuned by varying the Cu/Au ratio. This result suggests that Cu and Au atoms together constitute the surface active sites. The XPS results show that the surfaces of bimetallic samples are enriched in Au compared with the bulk composition (Table 1), and the surface composition varies with the Cu/Au ratio. The Cu and Au species on the alloy surface may serve as different active sites which favor the synergistic interaction,

Table 5. Effect of Reaction Temperature on the Hydrogenation of CALD Over Cu/SiO_2 and $6Cu\text{-}1.4Au/SiO_2$[a]

Catalyst	T (°C)	Time (min)	Conversion (%)	Selectivity (%)			Initial Rate[b]
				CALC	HALD	HALC	
$6Cu/SiO_2$	100	180	16	49	49	2	1.1
$6Cu/SiO_2$	110	120	19	44	53	3	2.0
$6Cu/SiO_2$	120	80	20	40	56	4	3.2
$6Cu/SiO_2$	130	50	20	37	60	3	5.1
$6Cu\text{-}1.4Au/SiO_2$	90	60	21	55	43	2	4.5
$6Cu\text{-}1.4Au/SiO_2$	100	30	20	52	46	2	8.6
$6Cu\text{-}1.4Au/SiO_2$	110	20	18	46	52	2	11.6
$6Cu\text{-}1.4Au/SiO_2$	120	12	19	43	54	3	20.4

[a]P_{H2} = 2 MPa; CALD = 1.5 mmol; stirring speed = 900 rpm.
[b]Initial reaction rate, mmol h^{-1} g_{cat}^{-1}.

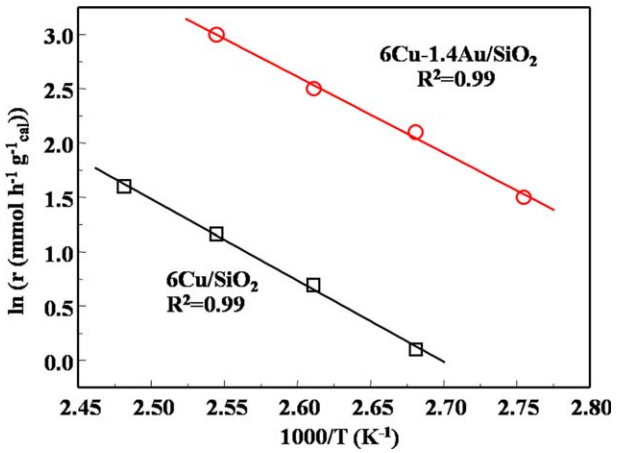

Figure 7. Arrhenius plots for the CALD hydrogenation over Cu/SiO_2 and 6Cu-1.4Au/SiO_2 catalysts.

[Color figure can be viewed in the online issue, which is available at wileyonlinelibrary.com.]

resulting in the enhanced catalytic activity as well as the variation in the catalytic performances with different Cu/Au contents.

As observed in the BE shift in the XPS profiles (Figure 5A), the electronic properties of Cu and Au are modified by alloying with each other, suggesting the electronic interaction between Cu and Au. According to the Pauling's electronegativity principles, Au is more electronegative than Cu. Thus, it is reasonably assumed that the electron transfers from Cu to Au in this bimetallic system, which is in accord with the literature.[18,23,32] The electron transferred from Cu to Au makes the surface Au electronically richness compared with Au atoms in monometallic catalyst. The AES results also show that the molar ratio of surface Cu^+/Cu^0 slightly increases by introducing Au species. The correlation between the selectivity of CALC and surface Cu^+/Cu^0 ratio of *x*Cu-*y*Au/SiO_2 is notable, implying that the Cu^+ sites are responsible for the selective hydrogenation of C=O bond, higher ratio of Cu^+/Cu^0 leads to higher selectivity of CALC. On the basis of our results and the literature, a possible schematic model of the catalysts is proposed and shown in Scheme 2.

The as-reduced Cu/SiO_2 catalyst has Cu^0 and Cu^+ species. It is accepted that the activation of H_2 takes place only on metallic surface,[51] thus Cu^0 is responsible for the dissociation of H_2. The FTIR spectra of chemisorbed CO results confirms that Cu^+ species is present on the surface of the metallic particles and reasonable deduction suggests that Cu^+ sites may be responsible for C=O adsorption.[52] Moreover, Volpe and coworkers[4] reported that Cu/MCM-48 were selective toward the hydrogenation of C=O bond in the CALD molecule due to the stabilization of Cu (I) species. Li and coworkers[53] investigated Cu/SiO_2 catalysts for propylene epoxidation with O_2, and found that the activation of the C=C bond on Cu^0 was easier than that on Cu^+. These findings indicate that the CALD interacts with Cu^+ site through the oxygen atom of the C=O group and interacts with Cu^0 site through the C=C group.

The as-reduced Au/SiO_2 catalyst has only Au^0 based on the XRD and XPS results. Our data have shown that the Au/SiO_2 catalyst leads to highly selective hydrogenation of C=C to produce HALD. The result is consistent with the previous reports.[46,48] It can be inferred that the Au^0 is responsible for the dissociation of H_2 and the CALD interacts with the Au^0 mainly through the C=C group.

The Cu-Au catalysts possess both Au-Cu alloys (Cu^0 and Au^0) and Cu^+. It is reported that the H_2 activation step is believed to be a key step in several hydrogenation reactions[49] and copper is less active than noble metals (Pt, Au, and Pd) in hydrogenation reactions.[54,55] Moreover, the introduction of Au species into the Cu/SiO_2 catalyst enhances H_2 activation ability (TPR results) and electronically enriched Au in Au-Cu alloy may donate electrons to hydrogen. Thus, the Au species of Au-Cu alloy is suggested to be responsible for the H_2 dissociation. It is also found that the particle size of the Cu-Au bimetallic catalyst is significantly smaller than that of monometallic Au catalyst, which should be one of the important reasons for the enhanced activity of the Cu-Au bimetallic catalyst. Indeed, Bus et al.[33,56] have demonstrated that H_2 dissociatively adsorbs only on the corners and edges of the supported gold. It is obvious that smaller gold particles having a higher fraction of low coordinated gold atoms

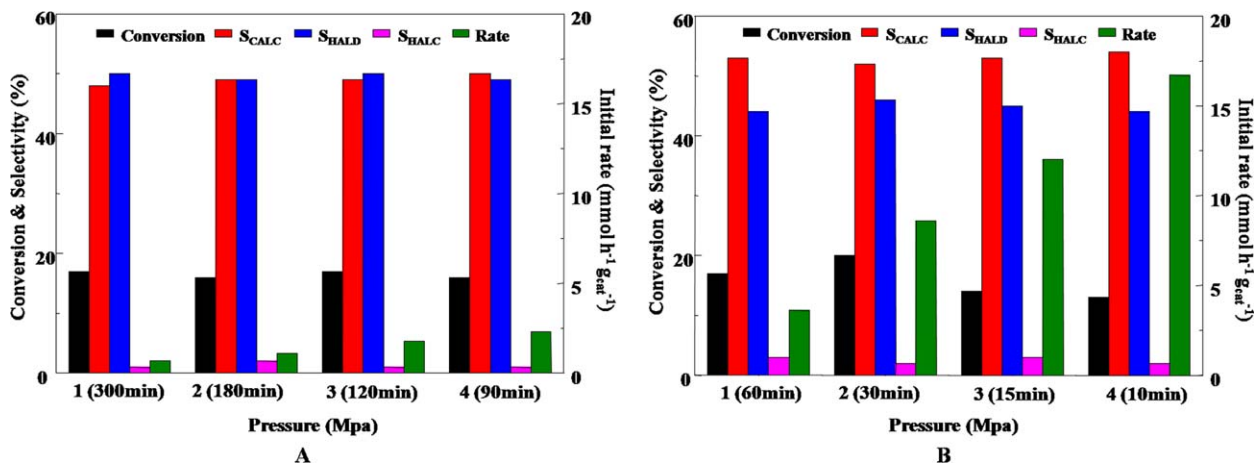

Figure 8. Effect of H_2 pressure on the hydrogenation of CALD over Cu/SiO_2 (A) and 6Cu-1.4Au/SiO_2 (B) (Reaction temperature = 100°C; CALD = 1.5 mmol; stirring speed = 900 rmp; reaction time in the bracket).

[Color figure can be viewed in the online issue, which is available at wileyonlinelibrary.com.]

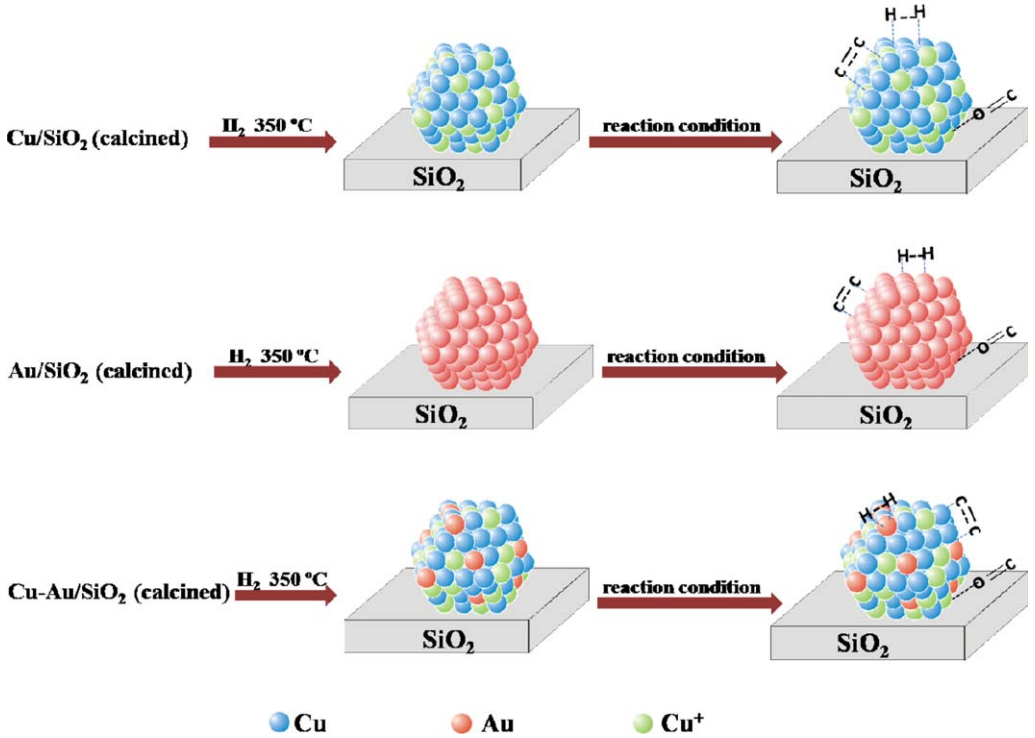

Scheme 2. Schematic illustration of the structural changes of the *x*Cu-*y*Au/SiO_2 under H_2 reduction condition and the possible mechanism of catalysis.

[Color figure can be viewed in the online issue, which is available at wileyonlinelibrary.com.]

present on corners and edges will have an increased average number of gold atoms active for hydrogen dissociation.[57,58] Due to electronic effects, the e^--sufficient Au sites may not adsorb the e^--rich C=C bond.[59] In addition, the experimental data show the correlation between the selectivity of CALC and the molar ratio of surface Cu^+/Cu^0 of *x*Cu-*y*Au/SiO_2, implying that the adsorption mode of CALD over Cu-Au/SiO_2 catalysts is the same as that of the Cu/SiO_2 catalyst. Thus, it can be concluded that the Au sites are responsible for the dissociative activation of H_2 molecules, whereas the Cu^0 and Cu^+ sites are, respectively, responsible for the adsorption-activation of C=C and C=O bond in the Cu-Au/SiO_2 bimetallic catalysts. As a result, highly dispersed synergistic Au-Cu alloy nanoparticles enhance the performance of CALD hydrogenation. However, excessively high gold loading, such as that in 6Cu-1.9Au/SiO_2, leads to relative large metallic particles and consequently decreases the catalytic ability compared with 6Cu-1.4Au/SiO_2.

Conclusions

In summary, we synthesized highly dispersed and uniform Cu-Au bimetallic catalyst via an ammonia-evaporation-deposition-precipitation method. The resultant Cu-Au/SiO_2 catalysts exhibited high activity for the CALD hydrogenation compared with monometallic Cu and Au catalysts. For example, the reaction rate for Cu/SiO_2 was as low as 1.1 mmol h^{-1} g_{cal}^{-1} and was enhanced to eightfold higher for 6Cu-1.4Au/SiO_2 catalyst with high selectivity of CALC (53%, at 55% of conversion). The activation energies of 6Cu/SiO_2 and 6Cu-1.4Au/SiO_2 catalysts calculated from Arrehenius plots were 62.2 ± 2.1 and 58.2 ± 2.6 kJ mol^{-1}, respectively. A synergistic effect between Cu and Au was proposed to explain the enhancements: the Au sites were responsible for the dissociative activation of H_2 molecules, and Cu^0 and Cu^+ sites contributed to the adsorption-activation of C=C and C=O bond, respectively. Based on these results, forming highly dispersed and uniform Au-Cu alloy nanoparticles resulted in a dramatic activity enhancement of Cu/SiO_2 for the CALD selective hydrogenation. Additionally, the reported catalyst is relatively potential for application in the reaction involving hydrogenation of C=C and C=O bonds. The results can guide the preparation or design of novel nanoalloy catalysts for the catalysis of selective hydrogenation reactions.

Acknowledgments

J.L.G. thanks the National Science Foundation of China (21006068), the Program for New Century Excellent Talents in University (NCET-10-0611), the Scientific Research Foundation for the Returned Overseas Chinese Scholars (MoE), and the Program of Introducing Talents of Discipline to Universities (B06006) for financial support. Y.H.Y. acknowledges the financial support from Ministry of Education, Singapore, academic research fund (AcRF) Tier 1 grants (RG 19/09 and RG 48/12).

Literature Cited

1. Claus P. Heterogeneously catalysed hydrogenation using gold catalysts. *Appl Catal A*. 2005;291(1–2):222–229.
2. Grosselin JM, Mercier C, Allmang G, Grass F. Selective hydrogenation of α,β-unsaturated aldehydes in aqueous organic two-phase solvent systems using ruthenium or rhodium complexes of sulfonated phosphines. *Organometallics*. 1991;10(7):2126–2133.
3. Mertens PGN, Vandezande P, Ye X, Poelman H, Vankelecom IFJ, De Vos DE. Recyclable Au^0, Ag^0 and Au^0–Ag^0 nanocolloids for the

chemoselective hydrogenation of α,β-unsaturated aldehydes and ketones to allylic alcohols. *Appl Catal A*. 2009;355(1–2):176–183.
4. Gutierrez V, Alvarez M, Volpe MA. Liquid phase selective hydrogenation of cinnamaldehyde over copper supported catalysts. *Appl Catal A*. 2012;413–414:358–365.
5. Nagaraja BM, Siva Kumar V, Shasikala V, Padmasri AH, Sreedhar B, David Raju B, Rama Rao KS. A highly efficient Cu/MgO catalyst for vapour phase hydrogenation of furfural to furfuryl alcohol. *Catal Commun*. 2003;4(6):287–293.
6. Maity P, Yamazoe S, Tsukuda T. Dendrimer-encapsulated copper cluster as a chemoselective and regenerable hydrogenation catalyst. *ACS Catal*. 2013;3(2):182–185.
7. Gutiérrez V, Nador F, Radivoy G, Volpe MA. Highly selective copper nanoparticles for the hydrogenation of α,β-unsaturated aldehydes in liquid phase. *Appl Catal A*. 2013;464–465:109–115.
8. Gutiérrez VS, Diez AS, Dennehy M, Volpe MA. Cu incorporated MCM-48 for the liquid phase hydrogenation of cinnamaldehyde. *Microporous Mesoporous Mater*. 2011;141(1–3):207–213.
9. Li X, Ai J, Li W, Li D. Ni-Co bimetallic catalyst for CH_4 reforming with CO2. *Front Chem Eng China*. 2010;4(4):476–480.
10. McCue A, Aponaviciute J, Wells RK, Anderson J. Gold modified cobalt-based Fischer-Tropsch catalysts for conversion of synthesis gas to liquid fuels. *Front Chem Sci Eng*. 2013;7(3):262–269.
11. Wang S, Zhang X, Zhao Y, Ge Y, Lv J, Wang B, Ma X. Pd-Fe/α-Al_2O_3/cordierite monolithic catalysts for the synthesis of dimethyl oxalate: effects of calcination and structure. *Front Chem Sci Eng*. 2012;6(3):259–269.
12. Liu X, Wang A, Wang X, Mou CY, Zhang T. Au-Cu alloy nanoparticles confined in SBA-15 as a highly efficient catalyst for CO oxidation. *Chem Commun*. 2008;27:3187–3189.
13. Ou TC, Chang FW, Roselin LS. Production of hydrogen via partial oxidation of methanol over bimetallic Au–Cu/TiO_2 catalysts. *J Mol Catal A: Chem*. 2008;293(1–2):8–16.
14. Chang FW, Ou TC, Roselin LS, Chen WS, Lai SC, Wu HM. Production of hydrogen by partial oxidation of methanol over bimetallic Au–Cu/TiO_2–Fe_2O_3 catalysts. *J Mol Catal A: Chem*. 2009;313(1–2):55–64.
15. Liu X, Wang A, Li L, Zhang T, Mou C, Lee J. Structural changes of Au–Cu bimetallic catalysts in CO oxidation: in situ XRD, EPR, XANES, and FT-IR characterizations. *J Catal*. 2011;278(2):288–296.
16. Li W, Wang A, Liu X, Zhang T. Silica-supported Au–Cu alloy nanoparticles as an efficient catalyst for selective oxidation of alcohols. *Appl Catal A*. 2012;433–434:146–151.
17. Li X, Fang SSS, Teo J, Foo YL, Borgna A, Lin M, Zhong Z. Activation and deactivation of Au–Cu/SBA-15 catalyst for preferential oxidation of CO in H_2-rich gas. *ACS Catal*. 2012;2(3):360–369.
18. Sugano Y, Shiraishi Y, Tsukamoto D, Ichikawa S, Tanaka S, Hirai T. Supported Au-Cu bimetallic alloy nanoparticles: an aerobic oxidation catalyst with regenerable activity by visible-light irradiation. *Angew Chem Int Ed*. 2013;52(20):5295–5299.
19. Chimentão RJ, Medina F, Fierro JLG, Llorca J, Sueiras JE, Cestero Y, Salagre P. Propene epoxidation by nitrous oxide over Au–Cu/TiO_2 alloy catalysts. *J Mol Catal A: Chem*. 2007;274(1–2):159–168.
20. Bracey CL, Ellis PR, Hutchings GJ. Application of copper-gold alloys in catalysis: current status and future perspectives. *Chem Soc Rev*. 2009;38(8):2231–2243.
21. Bracey CL, Carley AF, Edwards JK, Ellis PR, Hutchings GJ. Understanding the effect of thermal treatments on the structure of CuAu/SiO_2 catalysts and their performance in propene oxidation. *Catal Sci Technol*. 2011;1(1):76–85.
22. Gamboa-Rosales NK, Ayastuy JL, González-Marcos MP, Gutiérrez-Ortiz MA. Oxygen-enhanced water gas shift over ceria-supported Au–Cu bimetallic catalysts prepared by wet impregnation and deposition–precipitation. *Int J Hydrogen Energy*. 2012;37(8):7005–7016.
23. Yin A, Wen C, Dai W, Fan K. Nanocasting of CuAu alloy nanoparticles for methyl glycolate synthesis. *J Mater Chem*. 2011;21(25):8997–8999.
24. Wang Y, Duan X, Zheng J, Lin H, Yuan Y, Ariga H, Takakusagi S, Asakura K. Remarkable enhancement of Cu catalyst activity in hydrogenation of dimethyl oxalate to ethylene glycol using gold. *Catal Sci Technol*. 2012;2(8):1637–1639.
25. Zheng R, Porosoff MD, Weiner JL, Lu S, Zhu Y, Chen JG. Controlling hydrogenation of CO and CC bonds in cinnamaldehyde using silica supported Co-Pt and Cu-Pt bimetallic catalysts. *Appl Catal A*. 2012;419–420:126–132.
26. Shiraishi Y, Sakamoto H, Sugano Y, Ichikawa S, Hirai T. Pt-Cu bimetallic alloy nanoparticles supported on anatase TiO_2: highly active catalysts for aerobic oxidation driven by visible light. *ACS Nano*. 2013;7(10):9287–9297.
27. Murillo LE, Menning CA, Chen JG. Trend in the CC and CO bond hydrogenation of acrolein on Pt–M (M=Ni, Co, Cu) bimetallic surfaces. *J Catal*. 2009;268(2):335–342.
28. Kugai J, Miller JT, Guo N, Song C. Oxygen-enhanced water gas shift on ceria-supported Pd–Cu and Pt–Cu bimetallic catalysts. *J Catal*. 2011;277(1):46–53.
29. Rioux R, Vannice M. Dehydrogenation of isopropyl alcohol on carbon-supported Pt and Cu–Pt catalysts. *J Catal*. 2005;233(1):147–165.
30. Sitthisa S, Pham T, Prasomsri T, Sooknoi T, Mallinson RG, Resasco DE. Conversion of furfural and 2-methylpentanal on Pd/SiO_2 and Pd–Cu/SiO_2 catalysts. *J Catal*. 2011;280(1):17–27.
31. Fox EB, Velu S, Engelhard MH, Chin YH, Miller JT, Kropf J, Song C. Characterization of CeO_2-supported Cu–Pd bimetallic catalyst for the oxygen-assisted water–gas shift reaction. *J Catal*. 2008;260(2):358–370.
32. Gong J. Structure and surface chemistry of gold-based model catalysts. *Chem Rev*. 2012;112(5):2987–3054.
33. Bus E, Miller JT, van Bokhoven JA. Hydrogen chemisorption on Al_2O_3-supported gold catalysts. *J Phys Chem B*. 2005;109(30):14581–14587.
34. Corma A, Boronat M, Gonzalez S, Illas F. On the activation of molecular hydrogen by gold: a theoretical approximation to the nature of potential active sites. *Chem Commun*. 2007;32:3371–3373.
35. Boronat M, Concepción P, Corma A. Unravelling the nature of gold surface sites by combining IR spectroscopy and DFT calculations. *Implications in catalysis*. *J Phys Chem C*. 2009;113(38):16772–16784.
36. Zhang Y, Zheng N, Wang K, Zhang S, Wu J. Effect of copper nanoparticles dispersion on catalytic performance of Cu/SiO_2 catalyst for hydrogenation of dimethyl oxalate to ethylene glycol. *J Nanomater*. 2013;2013:1–6.
37. Jung J, Bae S, Lee W. Nitrate reduction by maghemite supported Cu-Pd bimetallic catalyst. *Appl Catal B*. 2012;127:148–158.
38. Epron F. Catalytic reduction of nitrate and nitrite on Pt–Cu/Al_2O_3 catalysts in aqueous solution: role of the interaction between copper and platinum in the reaction. *J Catal*. 2001;198(2):309–318.
39. Kim MJ, Na HJ, Lee KC, Yoo EA, Lee M. Preparation and characterization of Au-Ag and Au-Cu alloy nanoparticles in chloroform. *J Mater Chem*. 2003;13(7):1789–1792.
40. Hadjiivanov K, Knözinger H. FTIR study of CO and NO adsorption and coadsorption on a Cu/SiO_2 catalyst: probing the oxidation state of copper. *Phys Chem Chem Phys*. 2001;3(6):1132–1137.
41. Fisher IA, Bell AT. In situ infrared study of methanol synthesis from H_2/CO over Cu/SiO_2 and Cu/ZrO_2/SiO2. *J Catal*. 1998;178(1):153–173.
42. He Z, Lin H, He P, Yuan Y. Effect of boric oxide doping on the stability and activity of a Cu–SiO_2 catalyst for vapor-phase hydrogenation of dimethyl oxalate to ethylene glycol. *J Catal*. 2011;277(1):54–63.
43. Dandekar A, Vannice MA. Determination of the dispersion and surface oxidation states of supported Cu catalysts. *J Catal*. 1998;178(2):621–639.
44. Hong YC, Sun KQ, Zhang GR, Zhong RY, Xu BQ. Fully dispersed Pt entities on nano-Au dramatically enhance the activity of gold for chemoselective hydrogenation catalysis. *Chem Commun*. 2011;47(4):1300–1302.
45. Mäki-Arvela P, Hájek J, Salmi T, Murzin DY. Chemoselective hydrogenation of carbonyl compounds over heterogeneous catalysts. *Appl Catal A*. 2005;292:1–49.
46. Shi H, Xu N, Zhao D, Xu BQ. Immobilized PVA-stabilized gold nanoparticles on silica show an unusual selectivity in the hydrogenation of cinnamaldehyde. *Catal Commun*. 2008;9(10):1949–1954.
47. Chen HY, Chang CT, Chiang SJ, Liaw BJ, Chen YZ. Selective hydrogenation of crotonaldehyde in liquid-phase over Au/Mg_2AlO hydrotalcite catalysts. *Appl Catal A*. 2010;381(1–2):209–215.
48. Sun KQ, Hong YC, Zhang GR, Xu BQ. Synergy between Pt and Au in Pt-on-Au nanostructures for chemoselective hydrogenation catalysis. *ACS Catal*. 2011;1(10):1336–1346.
49. Serna P, Concepción P, Corma A. Design of highly active and chemoselective bimetallic gold–platinum hydrogenation catalysts through kinetic and isotopic studies. *J Catal*. 2009;265(1):19–25.

50. Gong J, Yue H, Zhao Y, Zhao S, Zhao L, Lv J, Wang S, Ma X. Synthesis of ethanol via syngas on Cu/SiO_2 catalysts with balanced Cu^0-Cu^+ sites. *J Am Chem Soc*. 2012;134(34):13922–13925.
51. Bradley RH. Surface studies of Cu/Cr/Ag impregnated microporous carbons. *Appl Surf Sci*. 1995;90:271–276.
52. Zheng J, Lin H, Wang Y, Zheng X, Duan X, Yuan Y. Efficient low-temperature selective hydrogenation of esters on bimetallic Au–Ag/SBA-15 catalyst. *J Catal*. 2013;297:110–118.
53. Su W, Wang S, Ying P, Feng Z, Li C. A molecular insight into propylene epoxidation on Cu/SiO_2 catalysts using O_2 as oxidant. *J Catal*. 2009;268(1):165–174.
54. Lenz J, Campo BC, Alvarez M, Volpe MA. Liquid phase hydrogenation of α,β-unsaturated aldehydes over gold supported on iron oxides. *J Catal*. 2009;267(1):50–56.
55. Campo B, Volpe M, Ivanova S, Touroude R. Selective hydrogenation of crotonaldehyde on Au/HSA-CeO_2 catalysts. *J Catal*. 2006; 242(1):162–171.
56. Bus E, van Bokhoven JA. Hydrogen chemisorption on supported platinum, gold, and platinum-gold-alloy catalysts. *Phys Chem Chem Phys*. 2007;9(22):2894–2902.
57. Boronat M, Illas F, Corma A. Active sites for H_2 adsorption and activation in Au/TiO_2 and the role of the support. *J Phys Chem A*. 2009;113(16):3750–3757.
58. Boronat M, Concepcion P, Corma A, Gonzalez S, Illas F, Serna P. A molecular mechanism for the chemoselective hydrogenation of substituted nitroaromatics with nanoparticles of gold on TiO_2 catalysts: a cooperative effect between gold and the support. *J Am Chem Soc*. 2007;129(51):16230–16237.
59. Rebelli J, Detwiler M, Ma S, Williams CT, Monnier JR. Synthesis and characterization of Au–Pd/SiO_2 bimetallic catalysts prepared by electroless deposition. *J Catal*. 2010;270(2):224–233.

Manuscript received Apr. 9, 2014, and revision received May 27, 2014.